

**Republic of Iraq
Ministry of Higher Education
and Scientific Research
University of Diyala
College of Science
Department of Physics**



**Synthesis and Characterization of PbS: Cd, Cu, Co
Nano composites Prepared by Pulsed Laser
Deposition For Gas Sensor Applications**

A Thesis

*Submitted to the Council of the College of Science- University of
Diyala in Partial Fulfillment of the Requirements for the Degree of
Doctor of Philosophy of Science in Physics*

By

Nawar Thamer Mohammed

B. Sc. in Physics-University of Diyala (2008-2009)

M. Sc. in Physics-University of Diyala (2013-2014)

Supervised By

**Assist. Prof. Dr.
Jasim .M. Mansoor**

***Prof. Dr.*
Kadhim. A.Aadim**

2022 AD

1444AH

بِسْمِ اللَّهِ الرَّحْمَنِ الرَّحِيمِ

قَالُوا سُبْحَانَكَ لَا عِلْمَ لَنَا إِلَّا مَا عَلَّمْتَنَا
إِنَّكَ أَنْتَ الْعَلِيمُ الْحَكِيمُ

البقرة [32]

صدق الله العظيم

Dedication

My PhD is dedicated to...

My parents.

My lovely wife.

My Son.....Mohammed.

My brothers and sister.

My uncle Dr. Mohammed

My supporters Friends

Nawar T. Mohammed

2022

Acknowledgement

First and foremost, I would like to thank Almighty Allah for giving me the strength, knowledge, ability and opportunity to undertake, persevere and complete this research. Without his blessings, this achievement would not have been possible.

There are many people I need to thank for their support and encouragement.

I would like to express my heartfelt thanks to my supervisors, *Assist. Prof. Dr. Jasim .M. Mansor* and *Prof. Dr. Kadhim. A.Aadim* , for their guidance, inspiration, and encouragement. I am very grateful for both their expertise and commitments throughout the course of my research.

Special thanks are extended to the University of Diyala, College of Science, specially the dean of College of Science, **Prof. Dr. Tahseen H. Mubarak** for his kind cooperation and constant support.

I express my thanks to head of Physics Department and all members, especially postgraduate faculty members and staffs of the college for their cooperation.

My sincere thanks are to *Prof. Dr. Ziad T. Khuthair* , for help, support and provide me with valuable scientific information during my research period.

It certainly would have been very difficult completing this research without the support from *my father, my mother, my wife , my brothers and my sister*. Their encouragements and supports inspired me to hold out to the end.

I would like to express my special thanks to my uncle *Dr.Mohammed Mirza* and my dearest friends (*Aiman & Dr.waled Al-zaidi*) to support me in my study.

I certainly cannot mention the names of everyone who contributed towards the success of this research, but as they have always known, I am very grateful.

Nawar T. Mohammed / 2022

Supervisors Certification

We certify that this thesis entitled " *Synthesis and Characterization of PbS: Cd, Cu, Co Nano composites Prepared by Pulsed Laser Deposition For Gas Sensor Applications* " for the student (**Nawar Thamer Mohammed**), was prepared under our supervisions at the Department of Physics, College of Science, University of Diyala in partial fulfillment of requirements needed to award the degree of *Doctor of Philosophy (Ph.D.) of Science in Physics*.

Signature:

Name: ***Dr. Jasim .M. Mansor***

Title: *Assist. Professor*

Address: College of Science

University of Diyala

Date: / / 2022

Signature:

Name: ***Dr. Kadhim. A.Aadim***

Title: *Professor*

Address: College of Science

University of Baghdad

Date: / / 2022

Head of the Physics Department

In view of available recommendation, I forward this thesis for debate by the examining committee.

Signature:

Name: ***Dr. Ammar A. Habeeb***

Title: *Assist. Professor*

Head of the Physics Department

Address: College of Science, University of Diyala

Date: / / 2022

Abstract

In this work, lead sulfide PbS thin films deposited on a glass substrate were mixed with (30, 50, and 70%) of cadmium, copper, and cobalt at room temperature. by use a pulsed laser deposition (PLD) technique, The laser energy was 600 mJ, and wave length 1064 nm. The number of laser pulses was fixedly set to 100 pulses for each ablation. The effect of mixing ratios on the structural and optical properties of PbS films were studied.

Using X-ray diffraction method, the structures of (PbS, PbS: Cd, PbS: Cu, and PbS: Co) thin films were investigated. X-ray analysis of the structure showed that it is polycrystalline and that the film's crystal system is the cubic system. also shows that the high intensity appeared at ($2\theta = 53.48886$ and 69.14403) and that the dominant trend of growth is (2 2 2) and (3 3 1), respectively and that the crystal size of the Pure PbS sample is (17.74 nm) and that the size of the crystal grows with the mixed ratio of (Cd, Cu, and Co).

The surface morphology of pure and mixed thin films deposited on a glass substrate by laser induced plasma technique at room temperature was examined by Field Emission Scanning Electron Microscope (FESEM).

FESEM micrographs for pure lead sulphide (PbS) and mixed (PbS: Cd, Cu, and Co) films deposited on glass substrates at various ratios it was noticed that the mixing of Cd, Cu and Co exhibits some changes in the PbS surface morphology in which the surface was found to be densely packed with crystallite.

For pure PbS thin film, it was observed that the film was dense, smooth, non-homogeneous with pinholes. Also, it was noted that the grains have a mixture of nano cauliflower and spherical-like shapes with different sizes. In addition, it was noted that PbS thin film formed was highly agglomerated.

FESEM micrographs of PbS thin film deposited with 30% of Cd, Cu, Co showed large clusters of spherical or semispherical shaped grains on some parts

of the images indicating an irregular growth rate of the grains. The images exhibited a dense compact of the grains covering the entire surface without any defects like cracks or pinholes. While the mixing ratios (50% and 70%) it was clearly observed that the mix ratio of cadmium increased the loss of the grain their sharp-edged nature and becomes smaller in size.

AFM measurements, which demonstrate that the films created using the PLD process, have In every instance, a dense surface for the thin films was achieved. The stacked grains made up the thin films.

From result of optical measurement by UV-ViS spectrophotometer showed that the thin films of (PbS, PbS:Cd, PbS:Cu, and PbS:Co) exhibit direct transit energy gap transitions. The absorbance of the films rises with the rising mixing ratio. The optical constants have been determined, including the absorption coefficient (α). As the mixing ratio is increased, the energy gap narrows.

Hall effect measurement showed that all the samples of (PbS , PbS:Cd , PbS:Cu and PbS:Co) were p- type conduction.

The gas sensor measurements showed that the resistivity of p- type gas sensor increases and return decreases by NO₂ Oxidization gas and decreases by high operation temperature . The sensitivity of all the samples decreased with increasing of mixing ratio because decreases the surface area with increase the grain size and the best sensor for NO₂ gas was the sample with a percentage of X = 30% Cu with a sensitivity of 355% at 150 °C .

	Contents	I
	List of Tables	VII
	List of Figures	IX
	List of Symbols	XIV
	List of abbreviations	XV
	Chapter One Introduction and Literature Review	
Item No	Subjects	Page no
1.1	Introduction	1
1.2	Thin Film Phenomena	2
1.3	Thin Film Applications	2
1.4.	Lead Sulphide (PbS)	3
1.5	Lead Sulphide applications	3-4
1.6	Cobalt	5
1.7.	Cadmium (Cd)	6
1.8	Copper (Cu)	8
1.9	Literature review	9
1.10	The Aim of the Work	17



	Chapter Two Theoretical part	
Item No	Subjects	Page no
2.1.	Introduction	18
2.2	The Film Deposition Techniques	18
2.3	Pulsed Laser Deposition Techniques (PLD)	19-20
2.4	Semiconductors	21
2.5	Crystal structure of semiconductors	22
2.5.1	Crystalline Semiconductors	22
2.5.1.1	Single Crystal Semiconductor	22
2.5.1.2	Polycrystalline semiconductor	23
2.5.2	Amorphous Semiconductors	23
2.6.	Semiconductor Compounds	24
2.7	.Energy Band Theory in Solid Materials	25
2.8	Crystal Defects	26
2.9	Structural Properties	28
2.9.1	X-Ray Diffraction (XRD)	28
2.9.1.1	Bragg's Law	29
2.9.2	Structure Parameters	31
2.9.2.1	Lattice Parameters	31
2.9.2.2	Crystallite Size (D)	31
2.9.2.3	Texture Coefficient (Tc)	31
2.9.2.4	Dislocation Density and Number of Crystals	32
2.10	Electronic Transitions	33



2.10.1	Direct Transition	33
2.10.2	Indirect Transitions	34
2.11	Optical Properties	36
2.11.1	The Interaction of Light With Semiconductor	36
2.11.2	Fundamental Absorption Edge	37
2.11.2.1	High Absorption Region	37
2.11.2.2	Exponential Absorption Region	38
2.11.2.3	Low Absorption Region	38
2.11.3	Transmittance	39
2.11.4	Absorbance	40
2.11.5	Reflectance	40
2.11.6	Optical Constants	41
2.11.6.1	Absorption Coefficient (α)	41
2.11.6.2	Refractive Index (n_0)	42
2.12	Hall Effect	43
2.13	Gas Sensor	44
2.13.1	Sensitivity (S)	44
2.13.2	Response and recovery times	45
2.13.3	Applications of Gas Sensors	46



	Chapter Three Experimental Work	
Item No	Subjects	Page No
3.1	Introduction	47
3.2	Equipment of Deposition	47
3.2.1	Nd:YAG Laser Source	48
3.2.2	Vacuum System	48
3.3	Target Preparation	49
3.4	Substrate Preparation	50
3.4.1	Glass substrates	50
3.5	Thin Films Deposition Procedure by PLD	50
3.6	The Techniques of Measurement	51
3.6.1	Measurement of Thickness	51
3.6.2	X-Ray Diffraction Analysis	52
3.6.3	Scanning Electron Microscope (SEM)	52
3.6.4	Atomic Force Microscope (AFM)	53
3.6.5	Optical Measurement	53
3.6.6	Electrical Measurement	54
3.6.6.1	Hall Effect	54
3.6.7	Gas Sensing Measurement	54
3.6.8	Procedure for Testing Sensors	55

Chapter Four Results and Discussion		
Item no	Subjects	Page No
4.1	Introduction	57
4.2	Structural Properties	57
4.2.1	X-Ray Diffraction (X-RD)	57
4.2.1.1	X-RD Diffraction of Pure PbS and mixed with (30%,50%,70%) Cd Thin Film	57
4.2.1.2	X-RD Diffraction of PbS mixed with (30%,50%,70%) Cu Thin Film	62-63
4.2.1.3	X-RD Diffraction of PbS mixed with (30%,50%,70%) Co Thin Film	67
4.2.1.4	Crystallites Size and FWHM of PbS mixed with Cd	71
4.2.1.5	Crystallites Size) and FWHM of PbS mixed with Cu	72
4.2.1.6	Crystallites Size and FWHM of PbS mixed with Co	73
4.3	Field Emission Scanning Electron Microscope (FESEM) and Energy Dispersive Spectrometer (EDS) Analysis	74
4.3.1	PbS pure and PbS mixed Cd	74
4.3.2	PbS pure and PbS mixed Cu	78
4.3.3	PbS pure and PbS mixed Co	83
4.4	Atomic Force Microscopy (AFM)	87



4.5	Optical Properties of PbS and PbS Mixed Cd Thin Films	93
4.5.1	The Absorbance	93
4.5.2	Absorption Coefficient	94
4.5.3	Energy Band gap	95
4.6	Optical Properties of PbS and PbS mixed Cu (PbS:Cu)	97
4.6.1	Absorbance	97
4.6.2	Absorption Coefficient	98
4.6.3	Optical bandgap	100
4.7	Optical Properties of PbS and PbS mixed Co (PbS:Co)	101
4.7.1	Absorbance	101
4.7.2	Absorption Coefficient	103
4.7.3	Energy gap	104
4.8	Hall Effect	106
4.9	Gas Sensing measurements of (PbS, PbS:Cd , PbS:Cu and PbS:Co)	107
4.9.1	Gas Sensing measurements of pure PbS and (PbS:Cd)	107
4.9.1.1	The resistance	107
4.9.1.2	The response and recover time	110
4.9.1.3	The Sensitivity	112
4.9.2	Gas Sensing measurements of pure PbS and (PbS:Cu)	114
4.9.2.1	The resistance	114
4.9.2.2	The response and recover time	119
4.9.2.3	The Sensitivity	120
4.9.3.	Gas Sensing measurements of pure PbS and (PbS:Co)	123
4.9.3.1	The resistance	123

4.9.3.2	The response and recover time	126
4.9.3.3	The Sensitivity	127
4-10	Conclusions	130
4-11	Suggestions for Future works	130

List of Tables

No.	Title	Page No.
1-1	Physical and chemical properties of Lead Sulphide	4
1-2	Physical and chemical properties of Cobalt	6
1-3	Physical and chemical properties of Cadimum	7
1-4	Physical and chemical properties of copper	9
2-1	Single and compound semiconductor	25
3-1	The mixing ratios and weight of PbS and (Cd, Cu and Co)	50
4-1	Crystalline parameters of PbS film prepared on a glass substrate according to the international label	57
4-2	Crystallite size and other parameters of pure PbS sample	59
4-3	Crystallite size and other parameters of PbS with mixed 30% Cd sample.	60
4-4	Crystallite size and other parameters of PbS mixed 50% Cd sample	61
4-5	Crystallite size and other parameters of PbS with mixed 70% Cd sample	62
4-6	Crystallite size and other parameters of PbS with mixed 30% Cu sample.	64
4-7	Crystallite size and other parameters of PbS mixed 50% Cu sample	65

4-8	Crystallite size and other parameters of PbS mixed 70% Cu sample	66
4-9	Crystallite size and other parameters of PbS mixed 30% Co sample	68
4-10	Crystallite size and other parameters of PbS mixed 50% Co sample.	69
4-11	Crystallite size and other parameters of PbS mixed 70% Co sample	70
4-12	grain size of prepared samples	76
4-13	Pb, S and Cd concentration in PbS, and PbS: Cd samples with various mix ratios	78
4-14	grain size of pure and mixed (PbS: Cu) thin films	80
4-15	Pb, S and Cu concentration in PbS, and PbS: Cu samples with various mix ratios.	83
4-16	grain size of pure and mixed (PbS: Co) thin films	85
4-17	Pb, S and Co concentration in PbS, and PbS: Co samples at various mix ratios	87
4-18	Surface roughness, root mean square (RMS) and grain size for pure and mixed thin films at different ratios of Cd	89
4-19	Surface roughness, root mean square (RMS) and grain size for pure and mixed thin films at different ratios of Cu	91
4-20	Surface roughness, root mean square (RMS) and grain size for pure and mixed thin films at different ratios of Co	93
4-21	Energy gap of pure film and mixed films at various ratios of Cd	96
4-22	Energy gap for pure film and mixed films by different ratios of Cu	100
4-23	Energy gap of pure film and mixed films at various ratios of Co	104
4-24	Hall parameters of (PbS) Pure and mixed films with 70% of Cd, Cu and Co	106

4-25	Response time , recover time and Sensitivity for Pure PbS and PbS:Cd	113
4-26	Response time , recover time and Sensitivity for for Pure PbS and PbS:Cu	122
4-27	Response time , recover time and Sensitivity for pure PbS and PbS:Co	129

List of Figures

No.	Title	Page No.
1-1	crystal structure of Lead Sulfide	3
1-2	crystal structure of Cobalt	5
1-3	crystal structure of Cadmium	7
1-4	crystal structure of Copper	8
2-1	diagram of thin film preparation techniques	19
2-2	Schematic diagram of PLD system	20
2-3	Scheme of energy bands in materials	22
2-4	crystal structure of material	24
2-5	The splitting of energy bands in diamond into permitted and forbidden energy bands	26
2-6	crystal defect	27
2-7	X-ray diagnosis	29
2-8	X-ray diffraction (XRD) of thin films	29
2-9	Crystal Levels and Braque's Law	30
2-10	Types of Electronic Transitions	35
2-11	absorption zones	39
2-12	Geometry of the Hall effect	44

2-13	Typical structure of a conductivity sensor	45
3-1	Pulse laser deposition system	47
3-2	Target before and after pressing	49
3-3	Schematic diagram of measurement of the films thickness	52
3-4	UV- Vis –Spectrophotometer	53
3-5	Electrical circuit of Hall Effect measurement	54
3-6	Gas sensor testing system	55
3-7	Schematic diagram of gas sensing and the electrical circuit setup	56
4-1	X-ray diffraction pattern of pure PbS and mixed with (30%,50%,70%) Cd thin film	58
4-2	X-ray diffraction pattern of pure PbS and mixed with (30%,50%,70%) Cu thin film	63
4-3	X-ray diffraction pattern of pure PbS and mixed with (30%,50%,70%) Co thin film	67
4-4	The relation between crystallite D with FWHM as a function Of mixing ratio of Cd	71
4-5	Histogram Diagan of PbS mixed Cd thin films at two different magnifications of (a) pure, (b) 30%, (c) 50% and (d) 70%	72
4-6	The relation between crystallite D with FWHM as a function Of mixing ratio of Co	73
4-7	FESEM images of PbS mixed Cu thin films at different magnification of (a) pure, (b) 30%, (c) 50% and (d)70%	75
4-8	Histogram Diagan of PbS mixed Cu thin films at two different magnifications of (a) pure, (b) 30%, (c) 50% and (d) 70%	76
4-9	EDS of the pure and PbS mixed Cu thin films at (a) pure, (b) 30%, (c) 50% and (d) 70%	77



4-10	FESEM images of PbS mixed Co thin films at different magnification of (a) pure, (b) 30%, (c) 50% and (d)70%.	79
4-11	Histogram Diagram of PbS mixed Co thin films at two different magnifications of (a) pure, (b) 30%, (c) 50% and (d) 70%	81
4-12	EDS of the pure and PbS mixed Co thin films at (a) pure, (b) 30%, (c) 50% and (d) 70%	82
4-13	FESEM images of PbS mixed Co thin films at different magnification of (a) pure PbS (b) 30%Co (c) 50%Co and (d) 70%Co	84
4-14	Histogram Diagram of PbS mixed Co thin films at two different magnifications of (a) pure PbS (b) 30%Co (c) 50%Co and (d) 70%Co	85
4-15	EDS of the pure and PbS mixed Co thin films at (a) pure PbS (b) 30%Co (c) 50%Co and (d) 70%Co	86
4-16	3D AFM images and histogram for PbS and mixed thin films of different ratios of Cd (a) pure PbS (b) 30%Cd (c) 50%Cd and (d) 70%Cd	88
4-17	3D AFM images and histogram for PbS and mixed thin films of different ratios of Cu (a) pure, (b) 30%, (c) 50% and (d) 70%	90
4-18	3D AFM images and histogram for PbS and mixed thin films of different ratios of Co (a) pure, (b) 30%, (c) 50% and (d) 70%	92
4-19	Absorbance versus wavelength of pure and mixed thin films at different ratios of Cd	94
4-20	The relation between absorption coefficient and wavelength of pure and mixed thin films at different ratios of Cd	95
4-21	The relation between $(\alpha h\nu)^2$ and $(h\nu)$ of pure and mixed thin films at different ratios of Cd	96
4-22	Absorbance versus wavelength of pure and mixed thin films at different ratios of Cu	98

4-23	The relation between absorption coefficient and wave length of pure and mixed thin films at different ratios of Cu	99
4-24	The relation between $(\alpha h\nu)^2$ and $(h\nu)$ of pure and mixed thin films at different ratios of Cu	101
4-25	Absorbance versus wavelength of pure and mixed thin films with different ratios of Co	102
4-26	The relation between absorption coefficient and photon energy of pure and mixed thin films at different ratios of Co	103
4-27	The relation between $(\alpha h\nu)^2$ and $(h\nu)$ of pure and mixed thin films at different ratios of Co	105
4-28	The variation of resistance with time at (150,200,250 and 300oC) for pure PbS	108
4-29	The variation of resistance with time at (250 and 300oC) for (PbS:0.3Cd)	109
4-30	The variation of resistance with time at (250 and 300oC) for (PbS:0.5Cd)	109
4-31	The variation of resistance with time at (250 and 300oC) for (PbS:0.7Cd)	110
4-32	The relation between response and recover time with operation temperature for (PbS , PbS:0.3Cd , PbS:0.5Cd and PbS:0.7Cd)	111
4-33	The sensitivity versus operation temperature for (PbS , PbS:0.3Cd , PbS:0.5Cd and PbS:0.7Cd).	112
4-34	The variation of resistance with time at (150,200,250 and 300oC) for pure PbS	115

4-35	The variation of resistance with time at (100 , 150 , 200 and 250oC) for (PbS:0.3Cu)	116
4-36	The variation of resistance with time at (100 , 150 , 200 and 250oC) for (PbS:0.5Cu)	117
4-37	The variation of resistance with time at (150 , 200 , 250 and 300oC) for (PbS:0.7Cu)	118
4-38	The relation between response and recover time with operation temperature for (PbS , PbS:0.3Cu , PbS:0.5Cu and PbS:0.7Cu)	120
4-39	The sensitivity versus operation temperature for (PbS , PbS:0.3Cu , PbS:0.5Cu and PbS:0.7Cu).	121
4-40	The variation of resistance with time at (150,200,250 and 300oC) for pure PbS	124
4-41	The variation of resistance with time at (250 and 300oC) for (PbS:0.5Co)	125
4-42	The variation of resistance with time at (150, 200, 250 and 300oC) for (PbS:0.7Co)	125
4-43	The relation between response and recover time with operation temperature for (PbS , PbS:0.5Co and PbS:0.7Co)	127
4-44	The sensitivity versus operation temperature for (PbS , PbS:0.5Co and PbS:0.7Co).	128

List of Symbols

Symbol	Meaning	Unit
E_g	Optical energy gap	eV
λ	The wavelength of the incident rays	(nm)
θ :	Brack diffraction angle in units.	degree
d_{hkl}	The distance between two successive levels in a crystal (hkl).	Å
a	Lattice constants	Å
hkl	Miller's coefficients	
K	shape factor	
β	Full Width at Half Maximum (FWHM)	radial
(Tc)	Texture Coefficient	
I (hkl)	Relative intensity of the plane (hkl).	
I_o (hkl)	Standard intensity of the level (hkl) taken from the ICDD card	
t	Thickness.	Å ^o
k	Space wave vector	
E_i	Initial energy of the electron in the valence	e.v
E_f	Final energy of the electron in the conduction bands	e.v
$h\nu$	Photon energy.	e.v
k_i	initial wave vector of the electron in the valence bands	
k_f	final wave vector of the electron in conduction bands	
q	Photon wave vector.	
r	An exponential parameter that specifies the type of transition	
B_o	A constant that depends on the nature of the substance	
α	Absorption coefficient.	
$h\nu$	The energy of a photon in units	e.v
r	An exponential coefficient that depends on the nature of the transition	
T	Transmittance	
n_o	Represents the true refractive index.	

K_0	Represents the damping factor.	
n_0	Refractive Index ()	
ϵ	Complex dielectric constant.	
ns	Refractive index of glass.	
Tc	Transmittance of glass.	
(VH)	Hall voltage	
(RH)	Hall coefficient	
(Bz)	Z-directional magnetic field	
μH	Mobility	
S%	Sensitivity (S)	

List of abbreviations

abbreviation	Meaning
PLD	Pulsed laser deposition
XRD	X-ray diffraction
CBD	chemical bath deposition
FE-SEM	Field-Emission Scanning Electron Microscopy
AFM	Atomic Force Microscope
FWHM	Full Width at Half Maximum
UV	Ultra Violet

Chapter One

Introduction and Literature Review

1.1.Introduction

Depending on the material's fixation ranges and the magnitude of the energy gap between the conduction band and the valence band, solids are categorized as conductors, insulators, or semiconductors. When the temperature rises from zero Kelvin (0K), when they are an insulating material, semiconductors exhibit great electrical conductivity. Because they are affordable, easily available, and influenced by magnetic, thermal, and light fields, semiconductors are widely used in electronic applications[1,2].

Chalcogenide semiconductors are regarded as Nano scale in part of nanotechnology due to its physical and chemical properties, which are mostly governed by their shape and size [3]. It is evident that the semiconducting nanomaterials' characteristics are controlled by their chemical composition, shape, and size [4]. Due to quantum size effects brought on by a predominate number, the semiconductor's nanostructure shows excellent electrical, photo magnetic, and photochemical characteristics that are distinct from those of micro-bulk materials. of atoms on surfaces of nanoscale materials [5]. Metal chalcogen transition compounds are important semiconductor materials, especially at their nanoscale, due to their excellent photo electronic transformation properties, potential applications in physics, chemistry, biology, medicine, materials science, and their various fields in fabrication of solar cells, sensitive sensors, and photon computers[6]. A few examples of the physical and chemical variables that sensors may detect or measure are temperature, pressure, sound, and concentration. and it transforms the information into an electrical signal that alerts us to the presence of anything, such as a harmful chemical or a high gas concentration[7].

1.2 Thin Film Phenomena

Thin film technology are very significant methods that has advanced the study of semiconductors. The study of materials in general and semiconductors in particular is the focus of the significant and distinctive field of thin-membrane physics, which is a subfield of solid state physics. Thin film technology has greatly aided the development of thin film manufacturing methods by providing a thorough understanding of its physical and chemical properties[8].

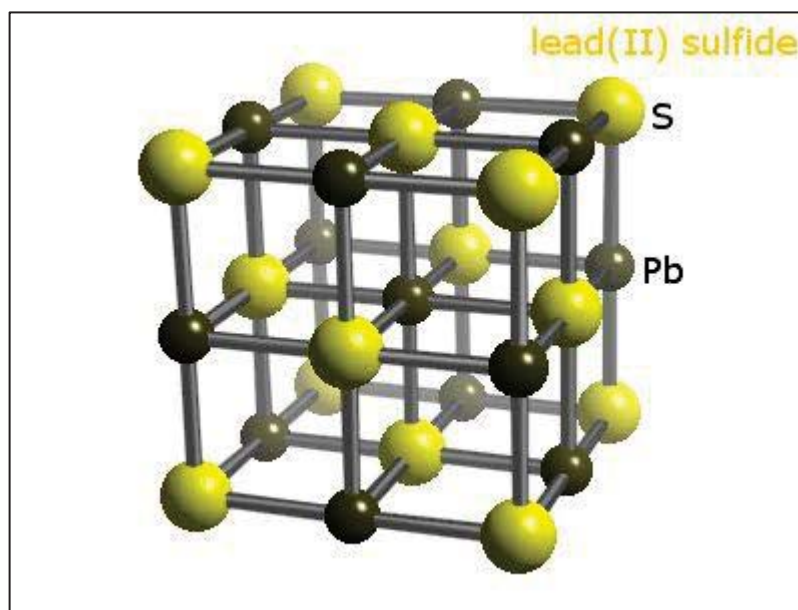
Thin films are composed of atoms in one or more layers with a maximum thickness of (one micrometer). According to the nature of the study, it must be placed on solid bases of glass, silicon, polymer, and other materials because it is thin and delicate (easily broken) [9].

1.3.Thin Film Applications

Resistors, capacitors, transistors, and other electronic components are made of thin films. Because of this character , these materials have a wide range of industrial uses. Advances in the thin film sector have largely been responsible for the accuracy and intelligence of all technologies that people utilize in electronic gadgets[10]. The development of thin films, namely those utilized in nanotechnology, allowed for their entry into the field and the examination of the properties of materials at the nanoscale scale[11].

1.4. Lead Sulphide (PbS)

Lead Sulphide is an IV-VI compound a class of semiconductor, materials that dominated in research and solid state technologies. The crystal structure of PbS is a cubic and as the figure (1-1) [12, 13].



Figure(1-1) crystal structure of Lead Sulfide [3]

1.5. Lead Sulphide applications

Thin film polycrystalline semiconductors have gained a lot of attention recently and used in a variety of electrical devices. The cheap cost of manufacture is the primary driver of this interest [14]. Infrared detectors, transistors, photoconductive cells, high temperature lubricants, and earthenware glazing all make use of this substance. In order to remove mercaptans from petroleum distillates, it is also utilized as a catalyst in the refinement of petroleum [15].

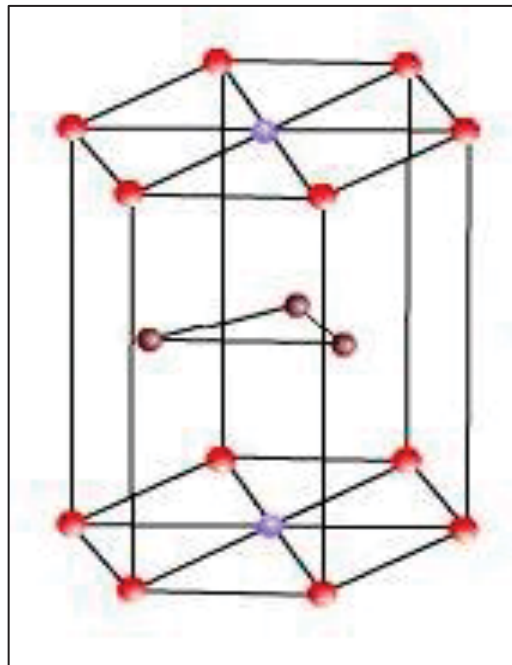
Table(1-1): physical and chemical properties of of Lead Sulphide[15]

Symbol.	PbS
Color	Black
Crystal structure	FCC
Moh's hardness	2.5
Molecular Wight (amu)	239.266
Density (g/cm ³)	7.60
Melting Point (°C)	1118
Boiling Point(°C)	1749
Lattice constant	5.936

By altering the grain size, the band gap of PbS may be changed dramatically. According to some reports, reducing the grain size to a nano domain can cause a rise in band gap from its bulk value by as much as 2.5 eV [16]. Additionally, the optical band gap of PbS thin films may be controlled (to 1.5 eV) and electrical resistivity can be reduced by altering various preparation conditions [17,18]. These features could be linked to substrate characteristics and growth circumstances. Due to these factors, several research teams have expressed a strong interest in creating and studying this material using a variety of deposition techniques, including electrode position, spray pyrolysis, photo-accelerated chemical deposition, microwave heating, and chemical bath deposition (CBD) [19], One of the most advanced and contemporary techniques for thin film deposition is pulsed laser deposition (PLD) .

1.6. Cobalt element

Close-packed hexagonal (Cph) and face-centered cubic crystal structures of cobalt have long been recognized (fcc). Both phases are capable of coexisting at ambient temperature, although the fcc structure is favoured thermodynamically at 450°C while the hcp phase is preferred at lower temperatures. The fcc form, however, seems to be favoured even below ambient temperature for tiny particles. Hull first discovered fcc and hcp cobalt in 1920 after studying the diffraction patterns of powders made using a variety of methods, but it observed new diffraction lines in samples made by spark erosion of bulk cobalt surfaces, but the structure was never fully established. It also noticed several new lines in the diffraction pattern of cobalt nanoclusters made by plasma evaporation and the subsequent condensation of the metal, but attributed these new lines to chance and the figure (1-3) showed the crystal structure of Cobalt and table (1-2) showed the physical and chemical properties of Cobalt [20].



Figure(1-2): crystal structure of Cobalt[20]

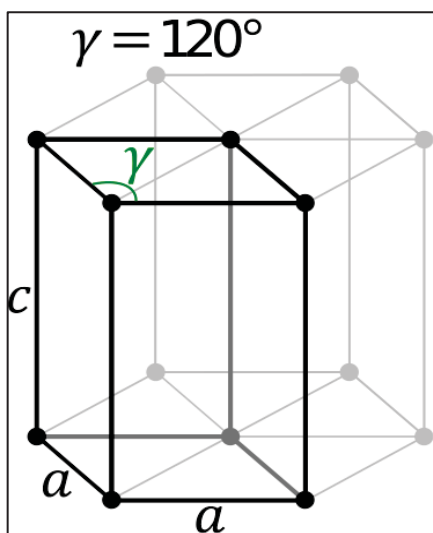
Table (1-2): physical and chemical properties of Cobalt [21]

Symbol.	Co
Color	silver-grey
Crystal structure	Fcc , hcp
Atomic number	27
Atomic Wight (amu)	58.933195
Density (g/cm ³)	8.9
Melting Point (°C)	1495
Boiling Point(°C)	2927
Atomic radius(Pm)	125

1.7. Cadmium element (Cd)

Cadmium is silvery-white, metal glossy, soft and ductile with a moderately high vapour pressure. Cadmium is produced during the mining of zinc metal ores include Cd, a divalent metal that is chemically similar to zinc and is present there due to isomorphous replacement. This metal is less prevalent than zinc and is frequently present in zinc ores as an impurity. It results from the mining of zinc. It is accessible in free form as soft, malleable, ductile, and moderately active similar to other stable metals Zinc and Mercury due to its oxidation state of +2 like Zinc and low melting point feature. In the Earth's crust, cd is a rare and equally distributed element with an average concentration of 0.15 to 0.2 mg/kg. The degree in which Cd is soluble in water depends on the acidity of the medium. As the acidity of the solution increases, more cadmium that is suspended or bonded to sediment will dissolve. In unpolluted fresh water, the

average Cd concentration is less than 0.001 mg/L, while in saltwater, it is 0.00015 mg/L. The figure (1-4) the image displayed the crystal structure of cadmium, and table (1-3) displayed its physical and chemical characteristics. Cadmium may enter plants through the roots or be aerosolized onto plant surfaces [22].



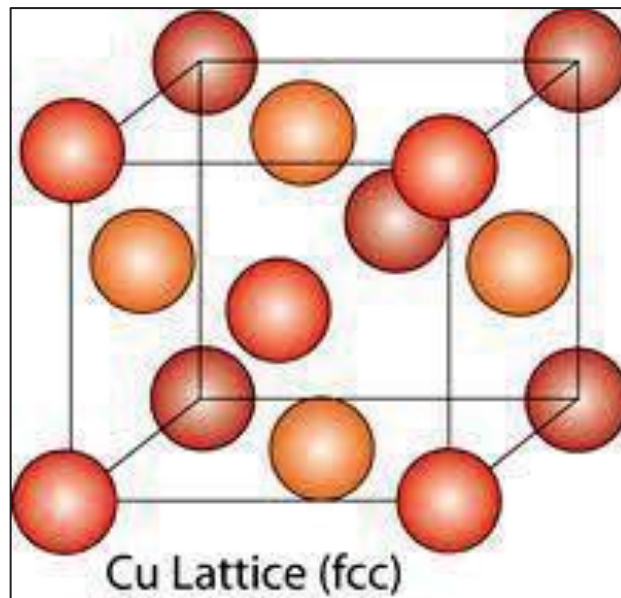
Figure(1-3) crystal structure of Cadmium[22]

Table(1-3) :physical and chemical properties of Cadimum [15]

Symbol.	Cd
Color	metallic
Crystal structure	closed-packed hexagonal
Atomic number	48
Atomic Wight (amu)	112.41
Density (g/cm ³)	8.69
Melting Point (°C)	321
Boiling Point(°C)	767
Atomic radius(Pm)	154

1.8. Copper element(Cu)

Copper, a reddish brown, malleable, ductile, highly electrically conductive, and corrosion-resistant metal, is typically present in metal ores that contain sulfides, arsenides, chlorides, and carbonates. Plumbing and electrical conductors are the principal uses for copper. It is typically has a +2 oxidation state. The black form of copper (II) oxide, known as CuO, may also be found in +1 state. Cu₂O is the chemical name for red copper (I) oxide. Copper functions as co-enzyme and is needed to life in trace levels. However it could be poison at high concentrations . Figure (1-5) shows the crystal structure of Copper and table (1-4) shows the physical and chemical properties of Copper[22] .



Figure(1-4) crystal structure of Copper [22]

Table (1-4) :physical and chemical properties of Copper [23]

Symbol.	Cu
Color	brown
Crystal structure	FCC
Atomic number	29
Atomic Wight (amu)	63.54
Density (g/cm ³)	8.94
Melting Point (°C)	1083
Boiling Point(°C)	2595
Atomic radius(Pm)	128

1.9.Literature review

Laxmi J. Tomar et. al. (2014) Synthesized PbS Nano crystals with rod shaped structure by chemical bath deposition process. The structure PbS was located using X-ray diffraction studies. The development of the cubic phase of PbS with the preferred orientation was indicated by the XRD data (2 0 0). The size of the typical crystallite was determined to be 7.82 nm. PbS nanorod production is verified by SEM pictures. By capturing absorption spectra in the wavelength range of 200-900 nm, the optical characteristics were investigated. The refractive index and optical band gap were discovered to be 1.47eV and 2.97, respectively. The electrical resistance was measured by four-probe way and determined to be 0.67MΩ [24].

Rajesh Kumar et. al. (2014) Synthesized nano crystalline PbS doped by Sb thin films were prepared by CBD method. The films were annealed for one hour at 673 K in the air after deposition. The X-ray diffraction (XRD) pattern of the films reveals the formation of well-crystallized PbS with a face-centered cubic structure and the preferred orientation (200). The average crystallite size was discovered to be between 40 and 43 nm. The average grain size, as determined by AFM surface research, is 52.3 nm with smooth surface. As a function of doping, the optical characteristics, absorbance, and transmission of the films have all been measured. A blue shift of the absorption edge in nanostructured thin films is satisfied by a decrease in the band gap E_g from 1.69 eV to 1.59 eV caused by increasing Sb doping in PbS thin films. The electrical resistivity of the films at room temperature ranged from 1.29 to 3.7×10^6 cm [25].

Mosiori et. al.(2014) synthesized Lead sulphide [PbS] thin films deposited by the [CBD] method on glass slide substrates for 120 minutes at room temperature. It is possible to model transmittance data in the 260–2000 nm wavelength range in order to derive additional optical and solid state parameters after using a spectrophotometer to assess the thin films' optical properties. The OJL model, the Drude model, and the Kronig Kramer Relation [KKR] model were three optical simulation models that were used by the software. As variables of wavelength and photon energy, the complex dielectric function, band gap, refractive index, absorbance, extinction, and absorption coefficients were examined. According to a study, PbS thin films were discovered to have a band gap of 0.88 eV, optical transmittance below 55% near infrared region, with significant absorption in visible range. It was made ideally for solar cells manufacturing [26].

S. SAGADEVAN et. al.(2014) synthesized lead sulphide (PbS) were Used the spin coating method, lead sulphide (PbS) was placed on a glass substrate while it was still warm. SEM is used to examine the particle size and shape, X-ray diffraction (XRD) was utilized to determine the structure and crystallite size of the films. In diverse frequency range of 50Hz-5MHz at various temperatures, the dielectric characteristics of PbS thin films were investigated. At various temperatures. Additionally, the electrical characteristics of the PbS thin films, such as their electronic polarizability and average energy gap or Penn gap, are computed [27].

Sanjeev Kumar et. al.(2015) studied the effect of substrate temperature on the structural and optical characteristics of PbS thin films produced by pulsed laser deposition. The main goal of this study was to raise many standards for high-caliber movies. At a substrate temperature of just 200°C, the experiment demonstrates the optimal orientation of the (200) reflection plane under compressive stress (-0.31211 GPa). However, an atomic force microscope can also be used to find the area of the film with the least amount of roughness. To calculate the band gap of these films in the weak absorption region, only reflectance spectra are used [28].

C. Rajashree et. al.(2015) investigated Cd doped PbS thin film properties by spray pyrolysis method. Glass substrates were doped with Cd at various concentrations (0, 2, 4, 6 and 8 at-%), and their characteristics were assessed. The X-ray diffraction (XRD) experiments revealed that all of the films exhibit face-centered cubic structure with a preferential orientation along the (2 0 0) plane, regardless of the Cd doping concentration. Optical tests show that when Cd concentration increases, the band gap of doped films shifts between 1.96 and 2.12 eV, and the film coated with 6 % Cd dopant has a maximum transmittance

of nearly 77%. Electrical measurements revealed a maximum conductivity of the 6 %Cd dopant-coated material. The PbS:Cd film coated with 6 %Cd dopant, as a consequence, enhanced the structural, morphological, optical, and electrical properties [29].

Yasmeen Z. Dawood et. al.(2015) studied the nano Lead sulfide PbS thin films' structural characteristics. The samples created via pulse laser deposition and applied on glass using laser intensity of 800mj at a 1064nm wavelength. By studying the impact of changing substrate temperature on these parameters. X-ray diffraction was used to identify the structural attributes of films. The films are highly crystallized, adhering to the substrate, and have a centered cubic structure with the preferred orientation (111), (200). When the film was deposited at a substrate temperature of 70 °C, the grain size was at its smallest value of 16.5 nm. The optical analysis revealed that direct transitions in the range of 1.55-2.45 eV were permitted depending on the substrate temperature [30].

F. Gode et. al.(2015) synthesized Lead sulfide thin films by Chemical bath deposition and utilized to deposit synthesized Lead sulfide thin films on glass substrates for two hours at room temperature. Different techniques were used to identified the thin films included X-ray diffraction, scanning electron microscopy, atomic force microscopy, optical absorption spectroscopy, and Hall effect measurements. Also, they studied the structure, surface morphology, optical, and electrical properties of these films. The produced films demonstrate the development of well-crystallized PbS with a cubic rock salt structure and the desired orientation (111) plane. The information of X-ray reflectivity from the atomic force microscopy image, showed that the lattice parameter and crystallite size of the films are $a = 600$ and 62 nm, respectively. The films' band

gap is thought to be 2.84 eV. The films' extinction coefficient, real and imaginary dielectric constant portions, and refractive index were assessed. According to the Hall measurements[31].

M. Chavez Portillo et. al.(2016) studied Li ion-doped PbS thin films' structural, electrical, and opto-electronic characteristics were researched. The Li inclusion in PbS led the crystal size to change from 36 nm to 12 nm, which was a substantial effect of the Li doping on crystallite size. The optical band gap in the range of 1.5e2.3 eV was changed as a result of Li inclusion. It was found that the Urbach energy depends on how much Li is incorporated and that there is Urbach tailing in the band gap. In SEM images, Li doping induced a discernible shift in grain size, although the morphology shifted from large grains to agglomerations of smaller grains. The electric conductivity of the films varied with the quantity of Li doping, reached a peak, and subsequently decreased for films with additional Li. Samples that have been doped showed greater photosensitivity[32].

Kadhim A. Aadim et. al.(2017) Used the pulsed laser deposition (PLD) method, to prepare thin films of lead sulfur (PbS) at room temperature and annealed at various temperatures (573, 673, and 773) K. PbS thin film structural measurements reveal face-centered cubic structure. The PbS surface was examined using atomic force microscopy (AFM). More uniformity may be seen in the movies. After annealing, the root mean square, average particle size, and surface roughness all increased. PbS thin films' optical characteristics are investigated in relation to wavelength in the range of (375 - 1100) nm. PbS thin films' optical transmittance showed that the transparency reduces as annealing temperature rises. Due to the formation of the crystallites, the direct energy gap for PbS thin films decreased with increasing annealing temperatures for all

samples. Calculations were also made for the optical constants such as the refractive index, extinction coefficient, and dielectric constant [33].

S. Ravishankar et. al.(2017) synthesized PbS and PbS with Fe doping were applied to glass substrates. On glass substrates, artificial PbS and Fe doped PbS thin films were created by spraying them with a perfume atomizer. This work investigates and reports on the effects of Fe doping concentration on the structural, morphological, optical, photoluminescence, and magnetic properties of PbS thin films. The changes in Fe concentration are 0, 1, 2, 3, and 4 wt%. Structural investigations reveal that the films all have a face-centered cubic crystal structure with a strong (200) preferred orientation. The Scherrer formula's projected crystallite size decreased with Fe doping, going from 55.73 nm to 31.97 nm. The elemental analysis result that the undoped and doped PbS thin films lack sulfur is considerably confirmed by the presence of an emission peak at 485 nm in the photoluminescence spectra. The optical band gap is blue-shifted by Fe doping. Doped PbS thin films had enhanced magnetic properties. The findings show that Fe²⁺ ions greatly enhanced the optical and magnetic properties of pure PbS thin films [34].

S. HOROZ et. al.(2018) synthesized PbS by chemical bath deposition (CBD) technique. X-ray diffraction (XRD), energy dispersive x-ray (EDX), and absorption measurements were used to investigate PbS which was produced via chemical bath deposition (CBD) method on glass substrates at ambient temperature. Although both thin films have the same structure, it was found that the particle size of the PbS:Ni (3%) thin film was smaller than that for PbS in the presence of Ni as additive material (cubic phase). Using the information gathered as a consequence of the optical measurements, a comparable outcome

was attained. Additionally, a bigger energy band gap was seen in the PbS thin film when Ni was added to it [35].

Hariyadi Soetedjo et. al.(2018) synthesized Cu-doped PbS thin films were prepared using a DC sputtering technique. The Cu dopant plate material was introduced directly onto the PbS sputtering target plate's surface to achieve the doping. According to SEM-EDX measurements, the Cu content in the PbS film was inversely correlated with the diameter of the Cu plate. The film was in crystalline cubic shape, according to the XRD pattern. According to the Hall effect test, Cu doping results in a considerable reduction in electrical resistivity and an increase in the carrier concentration to $3.55 \cdot 10^{19} \text{ cm}^{-3}$. The lowest resistivity measured was 0.13 at 18.5% Cu content. During deposition, (1 1 1) and (2 0 0) were oriented preferentially [36].

Omer Şahin et. al.(2019) studied the synthesized PbS and PbS:Mo(3%) thin films deposited using chemical bath deposition (CBD), a technique for producing pure PbS and PbS:Mo(3%) thin films on glass substrates. The major goal of this study was look at how the additional metal, Mo, can affect the optical energy band gap, photovoltaic characteristics, and crystallite size of the PbS semiconductor thin film. Even though the structure of the PbS:Mo(3%) thin film was the same as pure PbS, it was discovered to have a smaller crystallite size (24.12 nm) (25.97 nm). PbS and PbS:Mo(3%) thin films were found to have band gaps of 1.89 eV and 1.91 eV, respectively. The integration of Mo⁶⁺ ions into the PbS lattice is one potential explanation for the rise in the energy band gap of the PbS:Mo(3%) thin film. Via IPCE and J-V measurements, the photovoltaic characteristics of PbS and PbS:Mo(3%) thin films produced on Zn₂SnO₄ coated on FTO conductive glasses using CBD method were examined. At 400 nm, the pure PbS and PbS:Mo(3%) thin films' IPCE (%) values were 35% and 41%, respectively. For thin films constructed of pure PbS

and PbS:Mo(3%), the power conversion efficiency values were found to be 2.02% and 2.11%, respectively. It was found that the doped metal considerably enhanced the photovoltaic qualities of PbS thin films [37].

Mengting Liu et. al.(2019) prepared lead sulfide (PbS) thin films with Zn doping concentrations range from 0% to 5% by chemical bath deposition from previously investigated lead sulfide (PbS) thin films with Zn doping values ranging from 0% to 5%. According to X-ray diffraction, the predicted crystallite size reduced from 20.6 nm to 16.7 nm when zinc doping concentration rose (XRD). The PbS nanocrystals on the surface of the films had a pyramidal form, and FESEM images show that the grain size decreased as the doping concentration increased. The AFM measurements show that Zn doping has decreased the root mean square roughness of the PbS sheet. Using a UV-spectrophotometer in the 400-2400 nm range, PbS films' optical bandgap grew from 1.14 eV to 1.74 eV when their optical properties were investigated. All the films were p-type semiconductors at the time of deposition. [38].

Ahmed K.Abbas et. al.(2021) synthesized Lead sulfide Using laser-induced plasma. have been investigated by analyzing the laser-produced PbS plasma spectra at different energies (200, 300, 400, 500, 600mJ). The item was subjected to Nd: YAG laser light at a wavelength of 1064 nm. The electron temperature (T_e), electron density (n_e), Debye length (D), and plasma frequency were determined using optical emission spectroscopy (f_p). The analysis of this air mixture's spectra is a method that used to calculate the electron temperature by Boltzmann plot method and the electron density using the Stark broadening of Pb lines. The results showed the significance of electron temperature in the range of (1.465-1.599 eV) and electron density in the range of (1.11-1.47) 10^{18} cm^{-3} at a wavelength of (1064) nm [39].

1.10. The Aim of the Work

1- Study the effect of (cadmium, Copper, and Cobalt) in different mixing ratio on the (structural , optical and electrical) properties of PbS thin films prepared on glass substrates.

2- Manufacturing and preparing gas sensors from (PbS , PbS:Cd , PbS:Cu and PbS:Co)